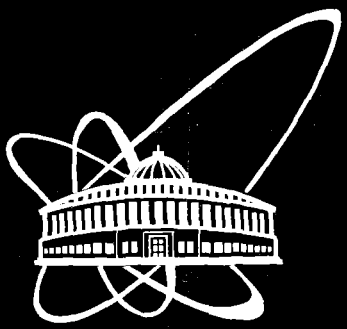

ОБЪЕДИНЕННЫЙ
ИНСТИТУТ
ЯДЕРНЫХ
ИССЛЕДОВАНИЙ

Дубна

E2-2003-83

G. N. Afanasiev*, V. G. Kartavenko, V. P. Zrelov

ON THE FINE STRUCTURE OF THE VAVILOV–CHERENKOV RADIATION

Submitted to «Physical Review E»

*E-mail: afanasiev@thsun1.jinr.ru

2003

1 Introduction

The classical Tamm-Frank theory [1] explaining the main properties of the Vavilov-Cherenkov (VC) effect [2,3] grounds on the assertion that a charge uniformly moving in medium with the velocity v greater than the light velocity in medium c_n radiates spherical waves from each point of its trajectory [4]. The envelope to these spherical waves propagating with the velocity c_n is the Cherenkov cone with a normal inclined under the angle θ_c towards the motion axis. Here $\cos\theta_c = 1/\beta_n, \beta_n = \beta n, \beta = v/c, c_n = c/n$ (c is the light velocity in vacuum and n is the medium refractive index).

The radiation of a charge uniformly moving in a finite medium space interval is usually studied in the framework of the so-called Tamm problem [5]. Under certain approximations (see below) Tamm obtained the remarkably simple formula which is frequently used by experimentalists for identification of the charge velocity.

In Refs. [6,7] the VC radiation observed in the Tamm problem was interpreted as interference of two bremsstrahlung (BS) shock waves arising at the beginning and at the end of motion.

On the other hand, the exact solution of the Tamm problem in the time representation was obtained in [8] for the dispersion-free medium. Its properties were investigated in some detail in [9,10]. It was shown there that side by side with BS shock waves the Cherenkov shock wave (CSW, for short) exists. According to [8-10], when a charge moves in the interval $(-z_0, z_0)$, the CSW is enclosed between the moving charge and the L_1 straight line originating from the $-z_0$ point corresponding to the beginning of motion and inclined under the angle θ_c towards the motion axis. The CSW is perpendicular to L_1. When a charge stops at the moment t_0, the CSW detaches from it and propagates between the L_1 straight line and the L_2 straight line originating from the z_0 point corresponding to the termination of motion and inclined under the same angle θ_c towards the motion axis. The positions of BS_1, BS_2 shock waves and the CSW are shown in Fig. 1(a). For an arbitrary moment of time $t > t_0$, the CSW is always tangential to both BS_1 and BS_2 shock waves. The length of CSW (coinciding with the distance between L_1 and L_2) is $L/\beta_n\gamma_n$, where $L = 2z_0$ is the motion interval and $\gamma_n = 1/\sqrt{|1-\beta_n^2|}$. As time goes, the CSW propagates between L_1 and L_2 with the light velocity in medium c_n (Fig. 1 (b)). The BS_1 and BS_2 shock waves are not shown in this figure. In the spectral representation (since transition to it involves the time integration) one gets space regions lying to the left of L_1 and to the right of L_2 to which BS_1 and BS_2 shock waves are confined, and the space region between L_1 and L_2 to which BS_1, BS_2 and CSW are confined. Let the measurements of the radiation intensity be made in the plane perpendicular to the motion axis z. Then, CSW cuts out in each of the $z = const$ planes the segment of the length $\delta\rho = L/\gamma_n$ independent of z, with its center at $R_0 = z/\gamma_n$ (Fig. 1 (c)). This picture refers to a particular $\phi = const$ plane (ϕ is the angle in the $z = const$ plane). Since the treated problem is the axially symmetrical one, the intersection of the CSW with $z = const$ plane looks like a ring with minor and major radii equal to $R_1 = R_0 - L/2\gamma_n$ and $R_2 = R_0 + L/2\gamma_n$, resp (Fig. 1 (d)). This qualitative consideration implies only the possible existence of the Cherenkov ring of the finite width. To find the distribution of the radiation intensity within and outside it, the numerical calculations are needed.

When the ratio of the motion interval to the observed wavelength is very large (this is a usual thing in the Cherenkov-like experiments), the Tamm formula has a sharp δ-

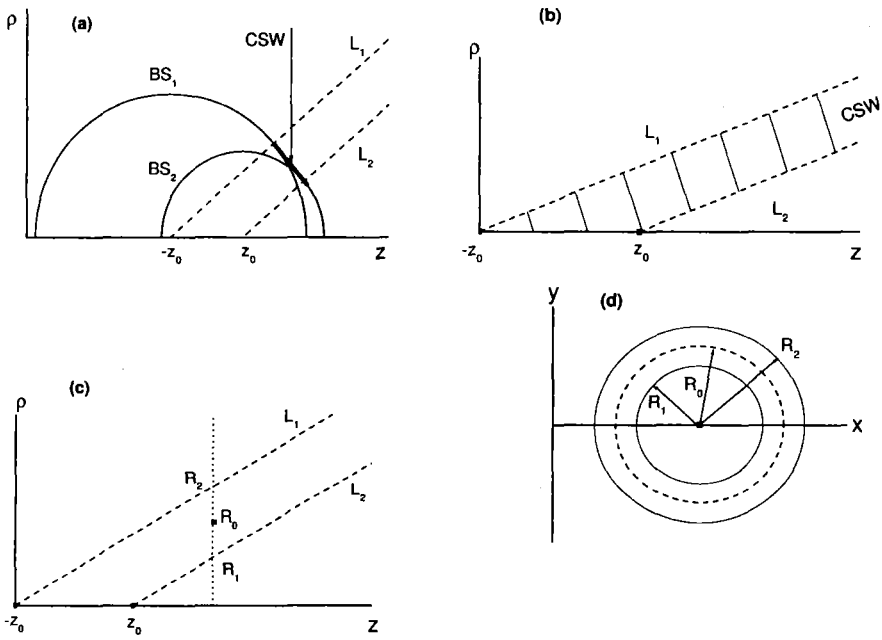

Figure 1: a): The position of the Cherenkov shock wave (CSW) and the bremsstrahlung ones arising at the beginning (BS_1) and the end (BS_2) of the charge motion at the fixed moment of time. The CSW is enclosed between L_1 and L_2 straight lines originating from the points corresponding to the boundaries of the motion interval; (b): The propagation of CSW between L_1 and L_2 straight lines; (c): In an arbitrary $z = const.$ plane perpendicular to the motion axis, the CSW , in the $\phi = const.$ plane, cuts off the segment of the same length $R_2 - R_1$ for any z; (d) Due to the axial symmetry of the problem, the CSW in the $z = const$ plane, cuts off the ring with internal and external radii R_1 and R_2, resp. The width $R_2 - R_1$ of the Cherenkov ring and the energy released in it do not depend on the observation plane position z.

type peak within the Cherenkov ring. Due to this, it cannot describe a rather uniform distribution of the radiation intensity inside the Cherenkov ring.

It should be mentioned that under the "shock waves" used throughout this paper we do not mean the usual shock waves used, e.g., in acoustics or hydrodynamics where they are the solutions of essentially nonlinear equations. The Maxwell equations describing the charge motion in medium are linear , yet, they can have solutions (when the charge velocity is greater than the light velocity in medium) with properties very similar to the true shock waves. For example, there is no electromagnetic field outside the Cherenkov cone, an infinite electromagnetic field on its surface and a rather smooth field inside the Cherenkov cone. The analog of the Cherenkov cone in acoustics is the Mach cone.

The observation of the above shock waves encounters certain difficulties when the used focusing devices collect radiation from the part of the charge trajectory lying inside the radiator into the sole ring, thus projecting the VC radiation and bremsstrahlung into the same place. The typical experimental setup with a lense radiator and the corresponding Cherenkov ring are shown in Fig. 2. In its left part, 1 means the proton beam with

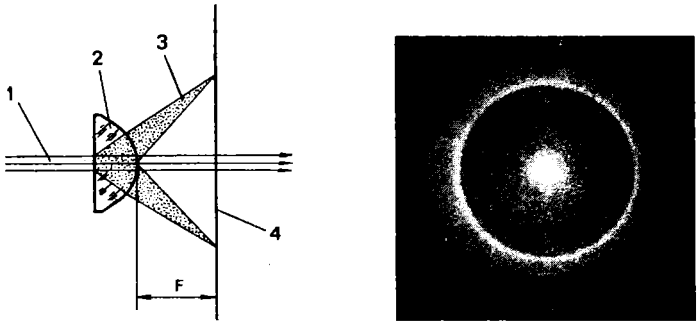

Figure 2: Left: The scheme of experiment with the lense radiator; 1 is the proton beam, 2 is the lense radiator, 3 is the focused VC radiation, 4 is the plane photofilm placed perpendicularly to the motion axis, F is the focal distance for paraxial rays; Right: the black-white photoprint from the photofilm shown on the left.

the energy 657 MeV and diameter 0.5 cm, 2 is the lense radiator with refractive index 1.512 and the focal distance 2.27 cm (for paraxial rays), 3 is the focused VC radiation ($\theta_{Ch} = 35.17^0$), 4 is a plane photofilm (18×24 cm). On the right side there is a black-white photoprint of the photofilm shown on the left. It has the form of a narrow ring.

To see how the VC radiation and bremsstrahlung are distributed in space, we turn to experiments in which the VC radiation was observed without using the focusing devices. These successful (although qualitative) experiments were performed by one of the authors (V.P. Zrelov, unpublished) in 1962 when preparing illustrations to monograph [11] devoted to the VC radiation and its applications. In this paper we processed these experimental data. The results are presented in the next section.

The plan of our exposition is as follows. The experiments mentioned above are dis-

cussed in section 2. The main computational formulae (exact and approximate) are collected in section 3. The analytic approximate formulae are needed for the qualitative analysis of the exact calculations. Radiation intensities for a number of observation plane positions are presented in section 4. In section 5, we discuss the results obtained and compare them with experimental data of section 2. Section 6 contains a brief summary and concrete proposals for the performance of new experiments.

2 Simple experiments with 657 MeV protons

2.1 The first 1962 experiment

The 657 MeV ($\beta = 0.80875$) proton beam of the phasotron of the JINR Laboratory of Nuclear Problems was used. The experimental setup is shown in Fig. 3. The collimated

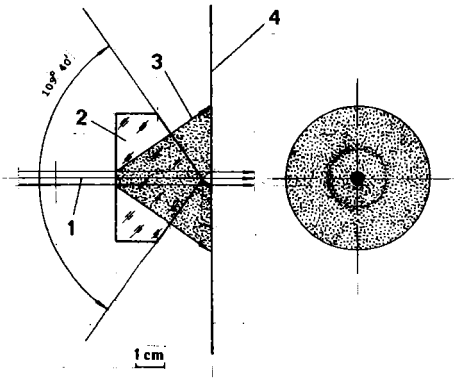

Figure 3: The experimental setup of the discussed experiment (Zrelov 1962). The proton beam (1) passing through the conical plexiglass radiator (2) induces the VC radiation (3, shaded region) propagating in the direction perpendicular to the cone surface. The observations are made in the plane photofilm (4) placed perpendicularly to the motion axis.

proton beam (1) with diameter 0.5 cm was directed to the conic polishing plexiglass radiator (2) ($n = 1.505$ for $\lambda = 4 \cdot 10^{-5}$ cm). The apex angle 109.7^0 of the cone enabled the VC radiation (3) to go out from the radiator in the direction perpendicular to the cone surface. The radiation was detected by the plane colour 18×24 cm photofilm placed perpendicularly to the beam at a distance of 0.3 cm from the cone apex. Nearly 10^{12} protons passed through the conical radiator. The black-white photoprint and the corresponding photometric curve (from which the beam background was subtracted) are shown in Figs. 4 (a) and (b), resp. The photometric curve describes the distribution

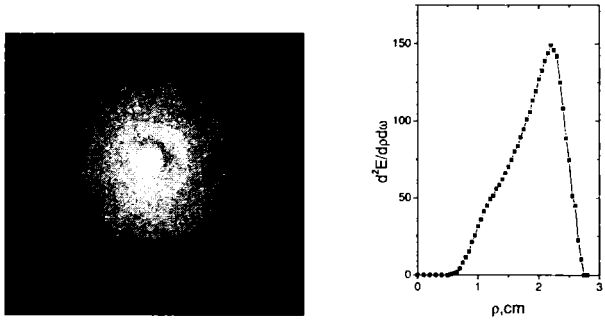

Figure 4: Left: The black-white photoprint from the photofilm shown in Fig. 3; Right: The photometric curve corresponding to the left part. One observes the increment of the radiation intensity at $\rho \approx 2.25cm$ which corresponds to the Cherenkov ray emitted from the point where the proton beam enters the radiator.

$d\mathcal{E}(\rho)/d\rho$ of the energy released inside the ring of the finite width. More accurately, $d\rho \cdot d\mathcal{E}(\rho)/d\rho$ is the energy released in the elementary ring with minor and major radii ρ and $\rho + d\rho$. resp. It is seen from this figure that the increment of the radiation intensity takes place at the radius $\rho = 2.25cm$ corresponding to the radiation emitted under the Cherenkov angle θ_c from the boundary point where the charge enters into the radiator.

2.2 The second 1962 experiment

In another experiment performed in the same 1962 year, the radiation intensity maxima corresponding to the radiation from the boundary points of the radiator are more pronounced. The experimental setup is shown in Fig. 5.

The radiator was chosen in the form of the crystalline quartz cube of side 1.5 cm. The proton beam (1) passed through the cube (2) along the axis connecting opposite vertices. In this case, the VC radiation went out through the three cube sides inclined under the angle $\psi = 35.26^0$ towards the motion axis. Likewise in the first experiment, the plane colour photofilm was placed perpendicularly to the beam axis, at a distance of $L = 2.35cm$ from the cube vertex. This guaranteed a smaller (as compared with a previous experiment) proton beam background in the VC radiation region. The direction of VC radiation rays (4) through one particular cube side G is shown. The black-white photoprint and the corresponding photometric curve measured along the direction "a-a" (Fig. 5) are shown in Fig. 6. To make the rough estimates, we averaged the crystalline quartz refractive index over ordinary and nonordinary wave vector directions, thus obtaining $n = 1.55$ for $\lambda = 5 \cdot 10^{-5}cm$. The corresponding Cherenkov angle was $\theta_c = 37.09^0$. In this case, the VC radiation rays emitted from the cube vertices should be at the radii $R_1 \approx 1.4cm$ and $R_2 \approx 2.3cm$ in the photofilm perpendicular to the motion axis. There is a rather pronounced radiation maximum in Fig. 6 only at $R_2 \approx 2.3cm$.

Theoretical consideration and numerical calculations presented below show that the just mentioned radiation intensity maxima should indeed take place and they are due to the discontinuities at the beginning and the end of the charge motion interval.

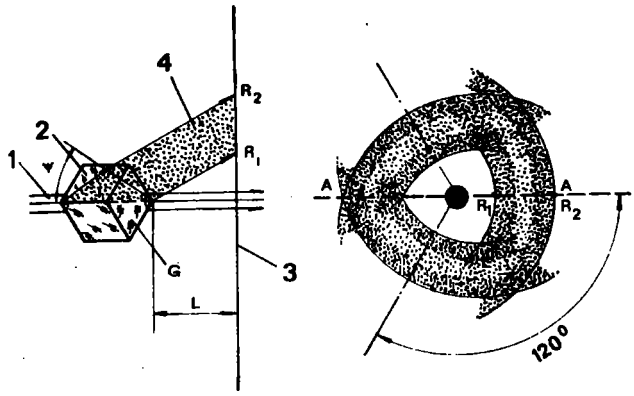

Figure 5: The experimental setup of another experiment (Zrelov 1962). The proton beam (1) propagates through the quartz cube (2) along the axis connecting the opposite cube vertices. The observations are made in the plane photofilm (3) placed behind the quartz cube perpendicularly to the motion axis; (4) is the direction of the Cherenkov rays passing through one of the cube sides.

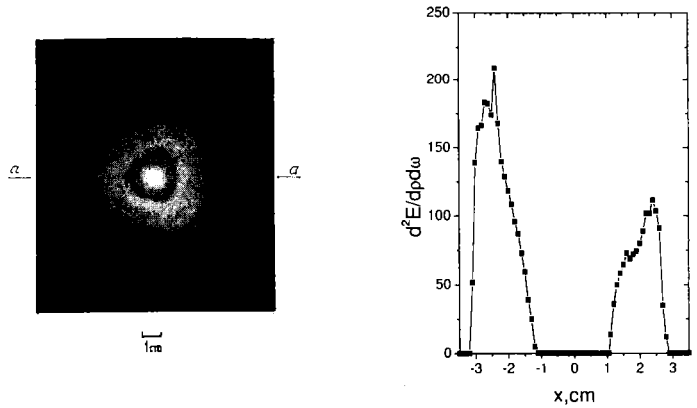

Figure 6: Left: The black-white photoprint from the photofilm shown in FIG. 5; Right: The photometric curve corresponding to the left part along the direction $a - a$; x means the distance along $a - a$. The increments of the radiation intensity at radii $R_2 \approx 2.3cm$ and $R_1 \approx 1.4cm$ corresponding to the Cherenkov rays emitted at the vertices where the beam enters and leaves the cube, resp. The radiation intensity for negative x describes the superposition of the VC radiations passing through two sides of cube (2). The radiation maxima relating to the ends of the Cherenkov rings are more pronounced than in Fig 4.

3 Main computational formulae

Formerly, the finite width of the Cherenkov rings on the observation sphere S of the finite radius r was studied numerically in [12], and analytically and numerically in [13]. It was shown there that the angle region to which the Cherenkov ring is confined, is large for small r and diminishes with its increasing. However, the width of the band corresponding to Cherenkov ring remains finite even for infinite values of r. Since the measurements in the discussed experiment were made in the plane perpendicular to the motion axis (which we identify with the z axis), we should adjust formulae obtained in [12,13] to the case treated.

3.1 The exact formula

In the spectral representation, the nonvanishing z component of the vector potential corresponding to the Tamm problem is given by

$$A_z(x,y,z) = \frac{e\mu}{2\pi c}\alpha_T, \tag{3.1}$$

where

$$\alpha_T = \int_{-z_0}^{z_0} \frac{dz'}{R}\exp(i\psi), \quad \psi = k(\frac{z'}{\beta} + nR), \quad R = [\rho^2 + (z-z')^2]^{1/2},$$

$$\rho^2 = x^2 + y^2, \quad k = \frac{\omega}{c}, \tag{3.2}$$

and μ is the magnetic permittivity (in the subsequent concrete calculations we always put $\mu = 1$).

The field strengths corresponding to this vector potential are

$$H_\phi = \frac{ekn\rho}{2\pi c}\int dz' \exp(i\psi)\frac{1}{R^2}(-i + \frac{1}{k_n R}),$$

$$E_\rho = \frac{iek\mu\rho}{2\pi c}\int dz' \exp(i\psi)\frac{z-z'}{R^3}(1 + \frac{3i}{k_n R} - \frac{3}{k_n^2 R^2}), \quad k_n = kn$$

(we do not write out the z component of the electric strength since it does not contribute to the z component of the energy flux which is of interest for us).

The energy flux emitted in the frequency interval $d\omega$ and passing through the circular ring with radii ρ and $\rho + d\rho$ lying in the $z = const$ plane is equal to

$$d\omega d\rho \frac{d^2\mathcal{E}}{d\rho d\omega},$$

where

$$\frac{d^2\mathcal{E}}{d\rho d\omega} = 2\pi\rho\frac{c}{2}(E_\rho H_\phi^* + c.c.) = \frac{e^2k^2n\mu\rho^3}{2\pi c}(I_c I_c' + I_s I_s'). \tag{3.3}$$

Here we put

$$I_c = \int dz' \frac{1}{R^2}(\cos\psi_1 - \frac{\sin\psi_1}{k_n R}), \quad I_c' = \int dz' \frac{z-z'}{R^3}[(1 - \frac{3}{k_n^2 R^2})\cos\psi_1 - 3\frac{\sin\psi_1}{k_n R}],$$

$$I_s = \int dz' \frac{1}{R^2}(\sin\psi_1 + \frac{\cos\psi_1}{k_n R}), \quad I_s' = \int dz' \frac{z-z'}{R^3}((1 - \frac{3}{k_n^2 R^2})\sin\psi_1 + 3\frac{\cos\psi_1}{k_n R}],$$

$$\psi_1 = \frac{kz'}{\beta} + k_n(R-r), \quad r^2 = \rho^2 + z^2.$$

3.2 The Tamm approximate formula

Imposing the conditions: i) $R >> z_0$ (this means that the observation distance is much larger than the motion interval); ii) $k_n R >> 1$, $k_n = \omega/c_n$ (this means that the observations are made in the wave zone); iii) $nz_0^2/2r\lambda << \pi$, $\lambda = 2\pi c/\omega$ (this means that the second-order terms in the expansion of R should be small compared with π since they enter into ψ_1 as a phase; λ is the observed wavelength), Tamm [7] obtained the following expression for the magnetic vector potential

$$A_z = \frac{e\mu}{\pi n\omega r}\exp(iknr)q, \quad q = \frac{1}{1/\beta_n - \cos\theta}\sin[\frac{kLn}{2}(\frac{1}{\beta_n} - \cos\theta)]. \tag{3.4}$$

Here $L = 2z_0$ is the motion interval and $\beta_n = \beta n$, $\beta = v/c$. Using this vector potential, one easily evaluates the quantity similar to (3.3)

$$S_z(T) = \frac{d^2\mathcal{E}}{d\rho d\omega}(T) = \frac{2e^2\mu z\rho^3}{\pi n c r^5}q^2, \tag{3.5}$$

where $\cos\theta = z/r$ and $r = \sqrt{\rho^2 + z^2}$. The value of (3.5) at $\cos\theta = 1/\beta_n$ is given by

$$S_z(T)|_{\cos\theta = 1/\beta_n} = \frac{e^2\mu k^2 L^2}{2\pi c n^4 \beta^5 \gamma_n^3 z}, \quad \gamma_n = \frac{1}{\sqrt{|1-\beta_n^2|}}. \tag{3.6}$$

For large kL, (3.5) is reduced to

$$S_z(T)|_{kL>>1} = \frac{e^2\mu kL}{c}(1 - \frac{1}{\beta_n^2})\delta(\rho - \frac{z}{\gamma_n}). \tag{3.7}$$

Integration over ρ gives the energy flux through entire $z = const$ plane

$$\frac{d\mathcal{E}}{d\omega}(TF) = \frac{e^2\mu kL}{c}(1 - \frac{1}{\beta_n^2}), \quad k = \frac{\omega}{c} \tag{3.8}$$

which is independent of z and coincides with the Tamm-Frank value [1] (as it should be).

Tamm himself evaluated the energy flux per unit solid angle and per unit frequency through the sphere of the infinite radius r

$$\frac{d^2\mathcal{E}}{d\Omega d\omega}(T) = \frac{e^2\mu}{\pi^2 nc}q^2\sin^2\theta. \tag{3.9}$$

This famous formula obtained by Tamm refers to the spectral representation and is frequently used by experimentalists for identification of the charge velocity.

3.3 The Fresnel approximation

This approximation is valid if the terms quadratic in z' in the development of R are taken into account while the cubic ones are neglected. The condition for the validity of the Fresnel approximation is $nz_0^3/2r^2\lambda << 1$. In this approximation,

$$\frac{d^2\mathcal{E}}{d\rho d\omega}(F) = \frac{e^2\mu k\rho z}{2cr^2}[(S_+ - S_-)^2 + (C_+ - C_-)^2]. \tag{3.10}$$

Here

$$C_\pm = C(z_\pm), \quad S_\pm = S(z_\pm), \quad z_\pm = \sqrt{\frac{k_n r}{2}}\sin\theta\left(\frac{1-\beta_n\cos\theta}{\beta_n\sin^2\theta} \pm \frac{z_0}{r}\right),$$

$C(x)$ and $S(x)$ are the Fresnel integrals defined as

$$S(x) = \sqrt{\frac{2}{\pi}}\int_0^x dt\sin t^2 \quad \text{and} \quad C(x) = \sqrt{\frac{2}{\pi}}\int_0^x dt\cos t^2.$$

From the asymptotic behaviour of the Fresnel integrals

$$S(x) \sim \frac{1}{2} - \frac{1}{\sqrt{2\pi}}\frac{\cos x^2}{x}, \quad C(x) \sim \frac{1}{2} + \frac{1}{\sqrt{2\pi}}\frac{\sin x^2}{x}$$

as $x \to \infty$ and their oddness ($C(-x) = -C(x)$, $S(-x) = -S(x)$) it follows that for large kr (3.10) has a kind of plato (if $\rho_2 - \rho_1 << \rho$)

$$\frac{e^2\mu k\rho z}{cr^2}, \tag{3.11}$$

for $\rho_1 < \rho < \rho_2$, where ρ_1 and ρ_2 are defined by the vanishing of the Fresnel integrals arguments. For $r >> z_0$, they are reduced to

$$\rho_{1,2} = \sqrt{\beta_n^2 - 1}(z \mp z_0).$$

Outside the plato, for the z fixed and $\rho \to \infty$, (3.10) decreases like $1/\rho^2$ coinciding with the Tamm formula (3.5). Mathematically, the existence of a plato is due to the fact that for $\rho_1 < \rho < \rho_2$ the Fresnel integral arguments z_+ and z_- have different signs. At the Cherenkov threshold ($\beta = 1/n$)

$$z_\pm = \sqrt{\frac{k_n r}{2}}\sin\theta\left(\frac{1}{2\cos^2(\theta/2)} \pm \frac{z_0}{r}\right)$$

have the same sign for $r > L$ and the radition intensity for $kr >> 1$ and $r > L$ should be small (as compared with the plato value (3.11)) everywhere.

These asymptotic expressions are not valid at $\rho = \rho_1$ and $\rho = \rho_2$. At these points the radiation intensities are obtained directly from (3.10)

$$\frac{d^2\mathcal{E}}{d\rho d\omega}(\rho = \rho_1) = \frac{e^2\mu k z\rho_1}{2cr_1^2}\{[C(\sqrt{\frac{2kn}{r_1}}z_0\sin\theta_1)]^2 + [S(\sqrt{\frac{2kn}{r_1}}z_0\sin\theta_1)]^2\},$$

$$\frac{d^2\mathcal{E}}{d\rho d\omega}(\rho=\rho_2)=\frac{e^2\mu nkz\rho_2}{2cr_2^2}\{[C(\sqrt{\frac{2kn}{r_2}}z_0\sin\theta_2)]^2+[S(\sqrt{\frac{2kn}{r_2}}z_0\sin\theta_2)]^2\}, \tag{3.12}$$

where r_1, r_2, θ_1 and θ_2 are defined as

$$r_1=\sqrt{\rho_1^2+z^2},\quad r_2=\sqrt{\rho_2^2+z^2},\quad \cos\theta_1=z/r_1,\quad \cos\theta_2=z/r_2.$$

For $kz_0^2/z >> 1$, one gets

$$\frac{d^2\mathcal{E}}{d\rho d\omega}(\rho=\rho_1)=\frac{e^2\mu kz\rho_1}{4cr_1^2},\quad \frac{d^2\mathcal{E}}{d\rho d\omega}(\rho=\rho_2)=\frac{e^2\mu nkz\rho_2}{4cr_2^2}, \tag{3.13}$$

that is four times smaller than (3.11) taken at the same points.
For $kz_0^2/r << 1$, the radiation intensity (3.10) outside the Cherenkov ring coincides with the one given by the Tamm formula (3.5).

3.3.1 Frequency distribution

Integrating (3.11) over ρ from ρ_1 to ρ_2 (suggesting that outside this interval, the radiation intensity (3.10) is negligible), one gets the frequency distribution of the radiated energy

$$\frac{d\mathcal{E}}{d\omega}(F)=\frac{e^2\mu kL}{c}(1-\frac{1}{\beta_n^2}),\quad k=\frac{\omega}{c}, \tag{3.14}$$

which coincides with the Tamm-Frank frequency distribution (3.8).

3.3.2 Energy radiated in the given frequency interval per unit radial distance

Integrating (3.11) over ω from ω_1 to ω_2, one gets the space distribution of the energy emitted in the frequency interval (ω_1,ω_2). It equals

$$\frac{d\mathcal{E}}{d\rho}(F)=\frac{e^2\mu\rho z}{2c^2r^2}(\omega_2^2-\omega_1^2) \tag{3.15}$$

for $\rho_1<\rho<\rho_2$ and zero outside this integral. When performing the ω integration, we disregarded the ω dependence of the refractive index n. This is valid for a rather narrow frequency interval.

The same conclusion is valid for (3.10) since the square bracket in it depends on ω only through the refractive index n. Integrating (3.10) over ω one gets

$$\frac{d\mathcal{E}}{d\rho}(F)=\frac{e^2\mu(\omega_2^2-\omega_1^2)\rho z}{4cr^2}[(S_+-S_-)^2+(C_+-C_-)^2]. \tag{3.16}$$

3.3.3 The total energy radiated in the given frequency interval

Integration of (3.14) over ω or (3.15) over ρ gives the total energy emitted in the frequency interval (ω_1,ω_2)

$$\mathcal{E}=\frac{e^2\mu L}{2c^2}(\omega_2^2-\omega_1^2)(1-\frac{1}{\beta_n^2}). \tag{3.17}$$

(Again, the medium dispersion is neglected).

3.4 Quasiclassical (WKB) approximation

To make easier the interpretation of the numerical calculations presented in the next section, we apply the quasiclassical approximation for the evaluation of the vector potential (3.1). For $\rho < (z - z_0)/\gamma_n$ and $\rho > (z + z_0)/\gamma_n$ (that is, below L_2 or above L_1) one gets

$$A_z(BS) = A_1(BS) - A_2(BS), \tag{3.18}$$

where

$$A_1(BS) = \frac{ie\mu\beta}{2\pi ck}\frac{1}{R_1}\exp(i\psi_1), \quad A_2(BS) = \frac{ie\mu\beta}{2\pi ck}\frac{1}{R_2}\exp(i\psi_2),$$

$$R_1 = \frac{1}{r_1 - \beta_n(z + z_0)}, \quad R_2 = \frac{1}{r_2 - \beta_n(z - z_0)}, \quad \psi_1 = k(nr_1 - \frac{z_0}{\beta}), \quad \psi_2 = k(nr_2 + \frac{z_0}{\beta}),$$

$$r_1 = \sqrt{\rho^2 + (z + z_0)^2}, \quad r_2 = \sqrt{\rho^2 + (z - z_0)^2}, \quad k = \frac{\omega}{c}.$$

It is seen that if $\beta > 1/n$, then A_z^{out} is infinite at $\rho = (z - z_0)/\gamma_n$ and $\rho = (z + z_0)/\gamma_n$, that is, at the border with CSW. There are no singularities in A_z^{out} for $\beta < 1/n$. Expanding r_1 and r_2 up to the first order in z_0 ($r_1 = r + z_0\cos\theta$, $r_2 = r - z_0\cos\theta$), one gets

$$A_z^T = \frac{e\mu q}{\pi cknr}\exp(iknr) \tag{3.19}$$

which coincides with the Tamm vector potential (3.4). Due to the approximations involved, the singularities of $A_1(BS)$ and $A_2(BS)$ compensate each other, and the Tamm vector potential (3.19) is finite at all angles. Thus, $A_z(BS)$ is the quasiclassical analogue of the Tamm vector potential.

On the other hand, in the space region $(z - z_0)/\gamma_n < \rho < (z + z_0)/\gamma_n$ (that is, between L_2 and L_1) one has

$$A_z = A_z(BS) + A_z(Ch), \tag{3.20}$$

where $A_z(BS)$ is the same as in (3.18) while

$$A_z(Ch) = \frac{e\mu}{2\pi c}\exp(i\psi_{Ch})\sqrt{\frac{2\pi\beta\gamma_n}{k\rho}}\Theta[\rho - (z - z_0)/\gamma_n]\Theta[(z + z_0)/\gamma_n - \rho], \tag{3.21}$$

where $\Theta(x)$ is the step function and

$$\psi_{Ch} = \frac{kz}{\beta} + \frac{\pi}{4} + \frac{k\rho}{\beta\gamma_n}.$$

It should be noted that $A_z(Ch)$ exists only if $\beta > 1/n$. Otherwise ($\beta < 1/n$), the vector potential is given by (3.18) in the whole angular region.

One can ask on what grounds we separated the vector potential into the Cherenkov ($A_z(Ch)$) and bremsstrahlung ($A_z(BS)$) parts? First, $A_1(BS)$ and $A_2(BS)$ exist below and above the Cherenkov threshold while $A_z(Ch)$ exists only above it. This is what intuitively expected for the VC radiation and bremsstrahlung. Second, $A_z(Ch)$ originates from the stationary point of the integral α_T (see Eq. (3.1)) lying inside the motion interval $(-z_0, z_0)$. For $A_1(BS)$ and $A_2(BS)$ the stationary points lie outside this interval, and their values are determined by its boundary ($\pm z_0$) points. Again, this is intuitively expected since the VC radiation is due to the charge radiation in the interval $(-z_0, z_0)$ while the

bremsstrahlung is determined by the points $(\mp z_0)$ corresponding to the beginning and the end of motion, resp. Third, to clarify the physical meaning of $A_z(Ch)$, we write out the vector potential corresponding to the unbounded charge motion. It equals

$$A_z = \frac{e\mu}{\pi c}\exp(\frac{ikz}{\beta})K_0(\frac{k\rho}{\beta\gamma_n})$$

for $\beta < 1/n$ and

$$A_z = \frac{i\epsilon\mu}{2c}\exp(\frac{ikz}{\beta})H_0^{(1)}(\frac{k\rho}{\beta\gamma_n}) \tag{3.22}$$

for $\beta > 1/n$. Since this vector potential tends to (3.21) as $\rho \to \infty$, $A_z(Ch)$ is a piece of the unbounded vector potential (3.22) confined to the $(z - z_0)/\gamma_n < \rho < (z + z_0)/\gamma_n$ region.

It is seen that for $kr \to \infty$, $A_z(BS)$ and $A_z(Ch)$ decrease like $1/kr$ and $1/\sqrt{kr}$, resp. This means that at large distances, $A_z(Ch)$ dominates in the $(z-z_0)/\gamma_n < \rho < (z+z_0)/\gamma_n$ region. Thus, A_z has a kind of plato inside this interval with infinite maxima at its ends (quasiclassics does not work at these points) and sharply decreases outside it. The corresponding quasiclassical field strengths are given by

$$E = E(BS) + E(Ch), \quad H = H(BS) + H(Ch), \tag{3.23}$$

$$H(BS) = H_1(BS) - H_2(BS), \quad E(BS) = E_1(BS) - E_2(BS),$$

$$H_1(BS) = \frac{e\beta\rho}{2\pi ckr_1R_1^2}(k_nR_1 + i)\exp(i\psi_1), \quad H_2(BS) = \frac{e\beta\rho}{2\pi ckr_2R_2^2}(k_nR_2 + i)\exp(i\psi_2)$$

$$E_1(BS) = -\frac{e\beta\rho}{2\pi c\epsilon k^2r_1^2R_1^2}\exp(i\psi_1)\times$$

$$\times[(1 - iknr_1)(1 - iknR_1)\frac{z + z_0}{r_1} + \frac{r_1}{R_1}(2 - iknR_1)(\frac{z + z_0}{r_1} - \beta_n)],$$

$$E_2(BS) = -\frac{e\beta\rho}{2\pi c\epsilon k^2r_2^2R_2^2}\exp(i\psi_2)\times$$

$$\times[(1 - iknr_2)(1 - iknR_2)\frac{z - z_0}{r_2} + \frac{r_2}{R_2}(2 - iknR_2)(\frac{z - z_0}{r_2} - \beta_n),]$$

$$H(Ch) = -\frac{e}{2\pi c}\sqrt{\frac{2\pi\beta\gamma_n}{k\rho}}\frac{1}{2\rho}(\frac{2ik\rho}{\beta\gamma_n} - 1)\exp(i\psi_{Ch}), \quad E(Ch) = \frac{1}{\epsilon\beta}H(Ch).$$

Here ϵ is the electric permittivity ($n^2 = \epsilon\mu$). It should be noted that when evaluating field strengths, we did not differentiate step functions entering into (3.21). If this were done, the δ functions at the ends of the Cherenkov ring appeared. Due to the breaking of the WKB approximation at these points, the vector potentials and field strengths are singular there and the inclusion of the just mentioned δ functions does not change anything. The energy flux along the motion axis is

$$S_z = \frac{d^2\mathcal{E}}{d\rho d\omega}(WKB) = \pi\rho c(EH^* + HE^*)\,. \tag{3.24}$$

In (3.23) and (3.24), $E \equiv E_\rho$ and $H \equiv H_\phi$ (in order not to overload formulae, we dropped the indices of E_ρ and H_ϕ).

We estimate the height of the plato to which mainly $H(Ch)$ and $E(Ch)$ contribute. It is given by

$$S_z(plato) = \pi\rho c[E(Ch)H^*(Ch) + H(Ch)E^*(Ch)] \approx \frac{e^2\mu k}{c\beta_n^2\gamma_n} \cdot \tag{3.25}$$

Since S_z is negligible outside this plato and since infinities at the ends of the Cherenkov ring are unphysical (they are due to the failure of the WKB method at these points) the frequency distribution is obtained by multiplying (3.25) by the width of the Cherenkov ring

$$\frac{d\mathcal{E}}{d\omega}(WKB) = \frac{e^2k\mu}{c\beta_n^2\gamma_n}\frac{L}{\gamma_n} = \frac{e^2\mu kL}{c}(1 - \frac{1}{\beta_n^2}). \tag{3.26}$$

This coincides with the Tamm-Frank formula (3.8). It is rather surprising that quite different angular distributions corresponding to the Tamm intensity (3.5), to the Fresnel one (3.10) and the quasiclassical one (3.24) give the same frequency distribution (3.8).

4 Numerical results

In Fig. 7, the radiation intensities are presented for various distances δz of the observation plane (δz is the distance from $z = z_0$ point corresponding to the termination of motion). We observe the qualitative agreement of the exact radiation intensity (3.3) with the Fresnel one (3.10). Both of them sharply disagree with the Tamm intensity (3.5) which does not contain the CSW responsible for the appearance of plato in (3.3) and (3.10). Fig. 7 (d) demonstrates that at large observation distances ($\delta z = 100cm$) the Tamm radiation intensity approaches the exact one outside the Cherenkov ring .

In Fig. 8, the magnified versions of exact radiation intensities corresponding to $\delta z = 0.3cm$ and $\delta z = 1cm$ are presented. In accordance with quasiclassical predictions, one sees the maxima at the ends of the $(z - z_0)/\gamma_n < \rho < (z + z_0)/\gamma_n$ interval. In Sec. 1 it was mentioned about the special optical devices focusing the rays directed under the Cherenkov angle into one ring. In the case treated, it is the plato shown in Figs. 7 and 8 and the BS peaks at its ends that are focused into this ring. The remaining part of BS will form the tails of the focused total radiation intensity. Probably, for such compressed radiation distribution the Tamm formula has a greater range of applicability.

5 Discussion

5.1 Vavilov-Cherenkov radiation and bremsstrahlung on the sphere

In the original and in nearly all subsequent publications on the Tamm problem, the radiation intensity was considered on the surface of the sphere of the radius r much larger than the motion interval $L = 2z_0$. It is easy to check that on the surface of the sphere of the finite radius r, the intervals

$$\rho > (z + z_0)/\gamma_n, \quad (z - z_0)/\gamma_n < \rho < (z + z_0)/\gamma_n \quad \text{and} \quad \rho < (z - z_0)/\gamma_n$$

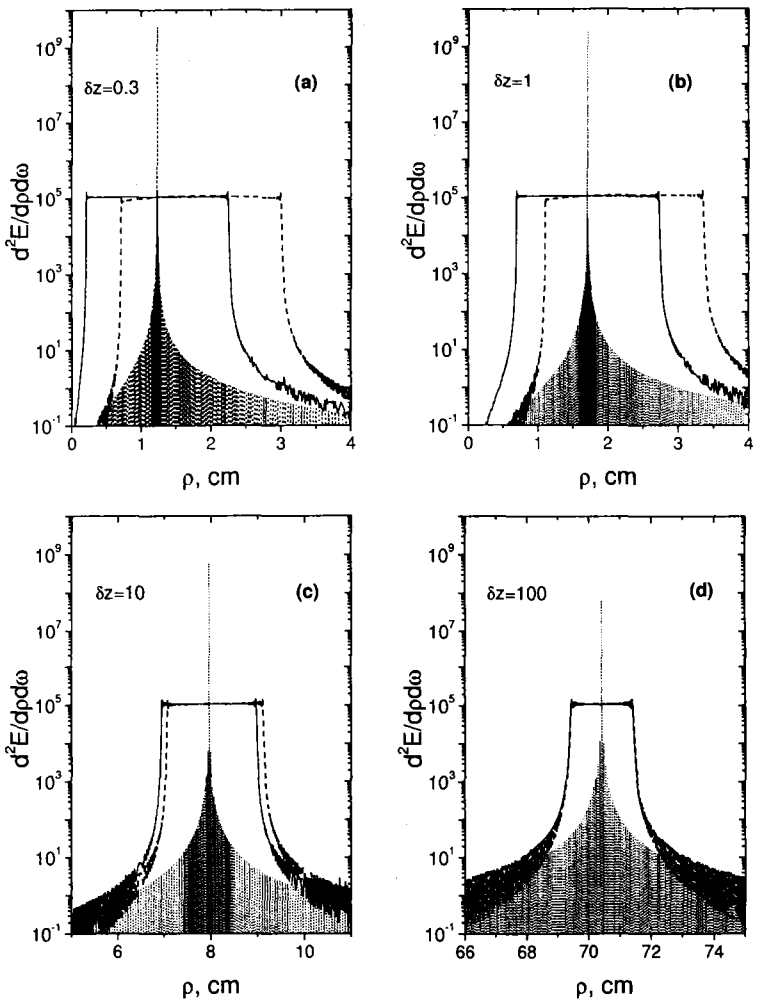

Figure 7: Theoretical radiation intensities in a number of planes perpendicular to the motion axis for the experimental setup shown in Fig. 3; δz means the distance (in cm) from the cone vertex to the observation plane. The solid, dashed, and dotted curves refer to the exact, Fresnel and Tamm intensities. In this figure and the following ones, the radiation intensities are in e^2/cz_0 units.

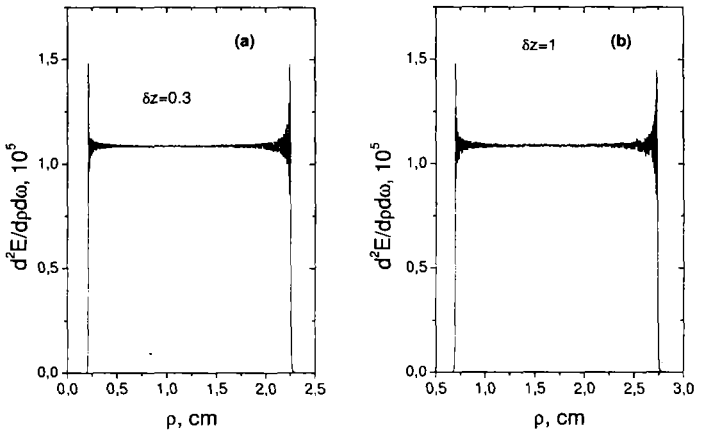

Figure 8: Exact theoretical radiation intensities in the $\delta z = 0.3cm$ and $\delta z = 1cm$ planes.

correspond to the angular intervals

$$\theta > \theta_1, \quad \theta_2 < \theta < \theta_1 \quad \text{and} \quad \theta < \theta_2,$$

where θ_1 and θ_2 are defined by

$$\cos\theta_1 = -\frac{\epsilon_0}{\beta_n^2\gamma_n^2} + \frac{1}{\beta_n}[1 - (\frac{\epsilon_0}{\beta_n\gamma_n})^2]^{1/2} \quad \text{and} \quad \cos\theta_2 = \frac{\epsilon_0}{\beta_n^2\gamma_n^2} + \frac{1}{\beta_n}[1 - (\frac{\epsilon_0}{\beta_n\gamma_n})^2]^{1/2}. \quad (5.1)$$

Here $\epsilon_0 = z_0/r$. For $r >> z_0$,

$$\theta_1 = \theta_c + \frac{\epsilon_0}{\beta_n\gamma_n}, \quad \theta_2 = \theta_c - \frac{\epsilon_0}{\beta_n\gamma_n},$$

where θ_c is defined by $\cos\theta_c = 1/\beta n$. In this case, the Tamm formula (3.9) is valid for $\theta < \theta_2$ and $\theta > \theta_1$, that is, nearly in the whole angular region. It should be added that the existence of the Cherenkov shock wave on the sphere is masked by the smallness of the angular region to which it is confined. It seems at first that on the observation sphere of infinite radius there is no room for CSW. This is not so. Although $\Delta\theta = \theta_1 - \theta_2 = 2\epsilon_0/\beta_n\gamma_n$ is very small for $r >> z_0$, the length of an arc corresponding to $\Delta\theta$ in a particular $\phi = const$ plane of the sphere S is finite: it is given by $\mathcal{L} = 2z_0/\beta_n\gamma_n$ and does not depend on the sphere radius r (for $r >> z_0$). Due to the axial symmetry of the problem, on the observation sphere S, the region to which the VC radiation is confined looks like a band of the finite width $\mathcal{L}$. Thus, the observation of the Cherenkov ring on the sphere is possible if the detector dimensions are much smaller than $\mathcal{L}$.

5.2 Vavilov-Cherenkov radiation and bremsstrahlung in the plane perpendicular to the motion axis

More pronounced the separation of the VC radiation and the BS looks in the plane perpendicular to the motion axis. We illustrate this using the quasiclassical intensities as

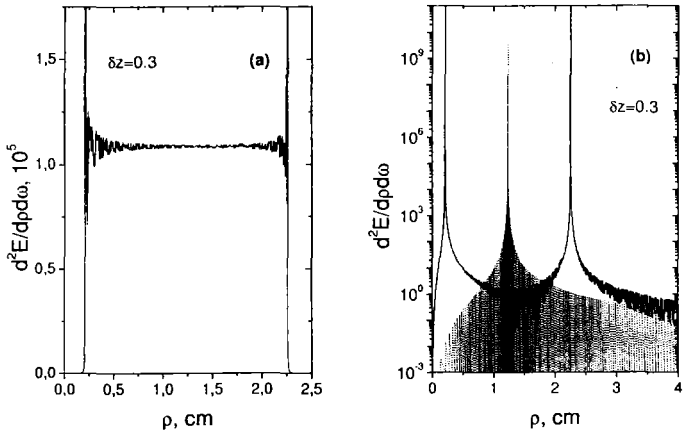

Figure 9: (a) Quasiclassical radiation intensity in the $\delta z = 0.3cm$ plane. It coincides with the exact one shown in Fig. 8 (a) everywhere except for the boundary points of the Cherenkov ring where the quasiclassical intensities are infinite due to the breaking of the WKB approximation; (b) The quasiclassical bremsstrahlung intensity (solid curve) and the Tamm one (dotted curve) in the $\delta z = 0.3cm$ plane. The sharp disagreement between them is observed.

an example. In Fig. 9 (a), we present the quasiclassical intensity (3.24) for $\delta z = 0.3cm$. We observe perfect agreement between it and the exact one shown in Fig. 8 (a) everywhere except for the boundaries of the region to which the VC radiation is confined. The quasiclassical approximation is unique in the sense that contributions of the VC radiation and the BS are clearly separated in the vector potential (3.20) and field strengths (3.23). To see the contribution of the BS, we omit $A_z(Ch)$, $E(Ch)$ and $H(Ch)$ in these relations by putting them to zero. The resulting intensity describing BS is shown in Fig. 9 (b). It sharply disagrees with the Tamm intensity (3.5). From the smallness of the BS intensity everywhere except for the boundaries of the Cherenkov ring it follows that oscillations of the total radiation intensity inside the Cherenkov ring are due to the interference of the VC radiation and the BS.

5.3 On the nature of the bremsstrahlung shock waves in the Tamm problem

Some words should be added on the nature of BS shock waves discussed above. In Refs. [6,7] they were associated with velocity jumps at the beginning and the end of motion. On the other hand, the smoothed Tamm problem was considered in [14] in the time representation. In it, the charge velocity v changes smoothly from zero up to some value $v_0 > c_n$ with which it moves in some time interval. Later, v decreases smoothly from v_0 to zero. It was shown in [14] that at the moment when v coincides with the light velocity in medium c_n, a complex arises consisting of the CSW with its apex attached to a moving charge, and the shock wave SW_1 closing the Cherenkov cone (and not coinciding with

shock wave originating at the beginning of motion). The inclination angle of the normal to SW_1 towards the motion axis (defining the direction in which SW_1 radiates) changes smoothly from 0 at the motion axis up to the Cherenkov angle θ_c at the point where SW_1 intersects the Cherenkov cone. Therefore, the radiation produced by the SW_1 fills the angular region $0 < \theta < \theta_c$. As time goes, the dimensions of the above complex grow since its apex moves with the velocity $v > c_n$, while the shock wave SW_1 propagates with the velocity c_n. Formerly, on the existence of radiation arising at the Cherenkov threshold and directed along the motion axis was pointed out by Tyapkin [15].

Since in the original Tamm problem the charge velocity changes instantly from 0 to v_0, the BS shock wave is in fact a mixture of these *three shock waves* having zero dimensions at the initial moment of time. Due to the specificity of the Tamm problem, the CSW and SW_1 are not separated in subsequent moments of time too. They are marked as CSW in Fig. 1 (a,b). The smoothed Tamm problem was also considered in [10] in the spectral representation. It was shown there that when a motion length along which a charge moves nonuniformly tends to zero, its contribution to the total radiation intensity also tends to zero. There are no velocity jumps for the smoothed problem and, therefore, the BS cannot be associated with instantaneous velocity jumps. However, there are acceleration jumps at the beginning and the end of motion and at the moments when the accelerated motion meets the uniform one. Thus, BS can still be associated with acceleration jumps. To clarify the situation, the Tamm problem with absolutely continuous charge motion (for which the velocity itself and all its time derivatives are absolutely continuous functions of time) was considered in [16]. It was shown there that a rather slow decrease in the radiation intensity outside the above plato is replaced by the exponential damping (formerly, for the charge motion in vacuum, the exponential damping for all angles was recognized in [17-20]). It follows from this that the authors [5,6] were not entirely wrong if under the BS shock waves used by them, one understands the mixture of three shock waves mentioned above and originating from the jumps of velocity, acceleration, other higher velocity time derivatives and from the transition of the medium light velocity barrier.

This is also confirmed by the consideration of radiation intensities for various charge velocities. Figure 10 (a) demonstrates that the position of the radiation intensity maximum approaches the motion axis, while its width diminishes as the charge velocity approaches the Cherenkov threshold ($\beta = 1/n \approx 0.665$). The radiation intensities presented in Fig. 10 (b) show their behaviour just above ($\beta = 0.67$) and below ($\beta = 0.66$) the Cherenkov threshold. It is seen that the maxima of the underthreshold and the overthreshold intensities differ by 10^5 times. Far from the maximum position, they approach each other. The radiation intensity at the Cherenkov threshold shown in Fig. 10 (c) is three orders smaller than the one corresponding to $\beta = 0.67$. The calculations in Figs. 10 (a-c) were performed using the Fresnel approximate intensity (3.10) which is in good agreement with the exact one (3.3) for the treated position ($\delta z = 10cm$) of the observation plane (as Fig. 7 demonstrates).

To see manifestly how the bremsstrahlung changes when one passes through the Cherenkov threshold, we present in Fig. 10 (d) the quasiclassical radiation BS intensities evaluated for $\beta = 0.67$ (in this case the VC radiation was removed by hand from (3.20) similarly as it was done for Fig. 9 (b)) and $\beta = 0.66$. The position of the observation plane is ($\delta z = 0.3cm$). Again, we observe the sharp decrease in the BS intensities in the

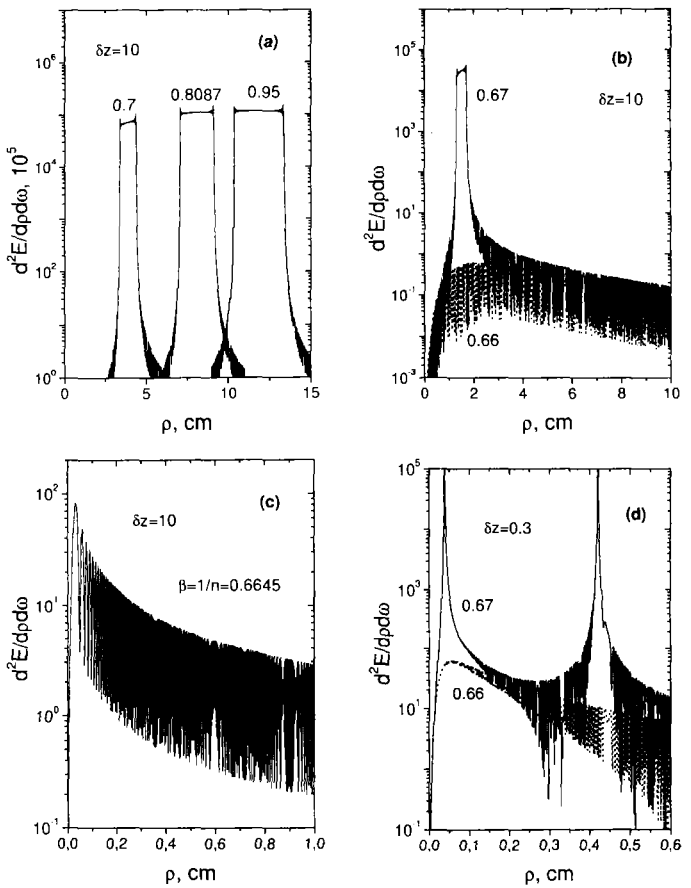

Figure 10: (a) Radiation intensities for a number of charge velocities above the Cherenkov threshold in the $\delta z = 10cm$ plane. As the charge velocity approaches the light velocity in medium, the position of the Cherenkov ring approaches the motion axis while its width diminishes; (b) Radiation intensities for the charge velocity slightly above and below the Cherenkov threshold in the $\delta z = 10cm$ plane; (c) Radiation intensities at the Cherenkov threshold in the $\delta z = 10cm$ plane. In accordance with theoretical predictions (see sect. (3.3)) it is much smaller than above the threshold; (d) Quasiclassical BS intensities for the charge velocity slightly above and below the Cherenkov threshold in the $\delta z = 0.3cm$ plane.

neighborhood of their maxima when one passes the Cherenkov barrier. This confirms that the BS shock waves used in [6,7] are the mixture of three shock waves mentioned above for the charge velocity above the Cherenkov threshold. For the charge velocity below the Cherenkov threshold, only the BS shock waves originating from the jumps of velocity, acceleration and other higher velocity time derivatives survive. They are much smaller than the singular shock wave originating when the charge velocity coincides with the medium light velocity.

5.4 Comparison with experiment

Turning to the comparison with experiment, we observe that it corresponds to the charge moving subsequently in air, in medium and, finally, again in air. The transition radiation which arises at the boundary of medium with air is approximately 100 times smaller than the VC radiation ([21,22]). Since the uniformly moving charge does not radiate in air where $\beta n < 1$ and radiates in medium where $\beta n > 1$, the observer inside the medium associates the radiation with instantaneous appearance and disappearance of a charge at the medium boundaries and with its uniform motion inside medium [4]. This justifies the applicability of the Tamm problem for the description of the discussed experiments.

Comparing theoretical intensities with the experimental ones we see that:
i) theoretical intensities have a plato (Figs. 7-10), while the experimental ones have a triangle form (Figs. 4,6); ii) the observed radiation peaks at the boundaries of the Cherenkov rings are not so pronounced as the predicted ones.

Probably, the triangle form of the observed radiation intensities is due to the smooth change of the charge velocity inside the dielectric. For such a motion, the radiation intensities obtained in [10,15,23] had indeed a triangle form. We estimate now the energy losses for the experiment treated. For the protons with energy 657 MeV, the energy ionization losses in plexiglass with density $\rho = 1.2 g/cm^3$ are $\Delta E/\Delta z = 2.91 MeV/cm$ [24]. This gives $\Delta E = 8.58 MeV$ for the radiator length 2.95 cm. The corresponding proton velocity change is $\Delta\beta = 2.3 \cdot 10^{-3}$. Alternatively, it can be associated with a smooth change of the refractive index at the border of vacuum and dielectric.

The item ii) can be understood if one takes into account that experiments mentioned in section 2 were performed with a relatively broad proton beam (0.5 cm in diameter). This leads to the smoothing of the boundary peaks after averaging over the proton beam diameter.

6 Conclusion

According to quantum theory [25], a charge uniformly moving in medium with the velocity greater than the light velocity in medium radiates γ quanta at the angle θ_c towards the motion axis ($\cos\theta_c = 1/\beta n$). It should be noted that for the uniform charge motion in unbounded medium, a photoplate placed perpendicularly to the motion axis will be darkened with the intensity proportional to $1/\rho$ (ρ is the distance from the motion axis) without any maximum at the Cherenkov angle. Despite its increase for small ρ, the energy emitted in a particular ring with the width $d\rho$ is independent of ρ. The surface of the cylinder coaxial with the motion axis will be uniformly darkened.

The Cherenkov ring can be observed only for the finite motion interval. In the $z = covst$ plane, the ring width is proportional to the charge motion interval L: $\Delta R = L/\gamma_n$ ($\gamma_n = 1/\sqrt{1-\beta_n^2}$, $\beta_n = \beta n$). It does not depend on the position z of the observation plane. The frequency dependence enters only through the refractive index n. The radiation emitted into a particular ring does not depend on z. For the fixed observation plane, the radiation intensity oscillates within the Cherenkov ring. These oscillations are due to the interference of bremsstrahlung and the Vavilov-Cherenkov radiation in (3.23). The large characteristic peaks at the ends of the Cherenkov ring are due to the bremsstrahlung shock waves which include shock waves originating from the jumps of velocity, acceleration, other higher velocity time derivatives and from the transition of the medium light velocity barrier. The finite width of the Cherenkov ring in the $z = const$ plane is due to the Cherenkov shock wave. Inside the Cherenkov ring ($R_1 < \rho < R_2$), the Tamm formula does not describes the radiation intensity at any position of the observation plane (see Fig. 7). Outside the Cherenkov ring ($\rho < R_1$ and $\rho > R_2$), the exact radiation intensity and the one given by the Tamm formula are rather small. In this angular region they approach each other at large distances satisfying $kz_0^2/r << 1$. For the experiments treated in the text, the l.h.s. of this equation equals unity at the distance $r \approx 1km$. On the other hand, the exact formula (3.3) describes the radiation intensity in all space regions.

We conclude: the experiments performed with a relatively broad 657 MeV proton beam passing through various radiators point to the existence of diffused radiation peaks at the boundary of the broad Cherenkov rings. This supports theoretical predictions [6, 7, 26, 27] on the existence of the shock waves arising when the charge motion begins and when the charge velocity coincides with the medium light velocity.

It is desirable to repeat experiments similar to those described in Section 2 with the charged particle beam of a smaller diameter ($\approx 0.1cm$), with a rather thick dielectric sample, without using the focusing devices and for various observation distances. This should result in appearance of more pronounced, just mentioned, radiation peaks.

References

[1] Tamm I.E. and Frank I.M., *Dokl. Akad. Nauk SSSR* **14** (1937) 107.

[2] Cherenkov P.A., *Dokl. Akad. Nauk SSSR* **2** (1934) 451.

[3] Vavilov S.I., *Dokl. Akad. Nauk SSSR* **2** (1934) 457.

[4] Frank I.M., *Vavilov-Cherenkov Radiation*, (Moscow, Nauka, 1988), in Russian.

[5] Tamm I.E., *J. Phys. USSR* **1** (1939) 439.

[6] Zrelov V.P. and Ruzicka J., *Czech. J. Phys.* **B39** (1989) 368.

[7] Zrelov V.P. and Ruzicka J., *Czech. J. Phys.* **42** (1992) 45.

[8] Afanasiev G.N., Beshtoev Kh. and Stepanovsky Yu.P., *Helv. Phys. Acta* **69** (1996) 111.

[9] Afanasiev G.N., Kartavenko V.G. and Stepanovsky Yu.P., *J. Phys. D* **32** (1999) 2029.

[10] Afanasiev G.N. and Shilov V.M., *J. Phys. D* **35** (2002) 854.

[11] Zrelov V.P., *Vavilov-Cherenkov Radiation in High-Energy Physics* (Jerusalaem, Israel Program for Scientific Translations, 1970)

[12] Afanasiev G.N., Kartavenko V.G. and Ruzicka J., *J. Phys. A* **33** (2000) 7585.

[13] Afanasiev G.N. and Shilov V.M., *J. Phys. D* **33** (2002) 2931.

[14] Afanasiev G.N. and Shilov V.M., *Physica Scripta* **62** (2000) 326.

[15] Tyapkin A.A., *JINR Rapid Communications* No 3(60)-93 (1993) 26.

[16] Afanasiev G.N., Shilov V.M. and Stepanovsky Yu.P., *Nuovo Cimento B* **117** (2002) 815.

[17] Abbasov I.I., *Kratkije soobchenija po fizike FIAN* No 1 (1982) 31; English translation: *Soviet Physics-Lebedev Institute Reports* No 1 (1982) 25.

[18] Abbasov I.I. *Kratkije soobchenija po fizike FIAN* No 8 (1985) 33; English translation: *Soviet Physics-Lebedev Institute Reports* No 8 (1985) 36.

[19] Abbasov I.I, Bolotovskii B.M. and Davydov V.A., *Usp. Fiz. Nauk* **149** (1986) 709. English translation: *Sov. Phys. Usp.* **29** (1986) 788.

[20] Bolotovskii B.M. and Davydov V.A., *Izv. Vuzov, Radiofizika* No 1 (1981) 31.

[21] Ruzicka J. and Zrelov V.P., *Nucl. Instrum. Methods* **165** (1979) 307

[22] Hrmo A. and Ruzicka J., *Nucl. Instrum. Methods* **A451** (2000) 506

[23] Afanasiev G.N., Kartavenko V.G. and Zrelov V.P., *JINR preprint*, E2-2001-207 (2001) Dubna.

[24] Janni J.F., *Atomic data and nuclear data tables* **27** (1982) 284.

[25] Ginsburg V.L., *Zhurnal Eksp. Theor. Phys.* **10** (1940) 589.

[26] Afanasiev G.N., Eliseev S.M. and Stepanovsky Yu.P., *Proc. Roy. Soc. London* **A454** (1998) 1049.

[27] Afanasiev G.N. and Kartavenko V.G., *Can. J. Phys.* **77** (1999) 561.

Received on April 25, 2003.

Афанасьев Г. Н., Картавенко В. Г., Зрелов В. П. E2-2003-83
О тонкой структуре излучения Вавилова–Черенкова

С целью изучения тонкой структуры черенковских колец проанализированы эксперименты (Зрелов В. П.), в которых черенковское излучение регистрировалось без использования фокусирующих устройств. При этом в плоскости, перпендикулярной оси движения протонов, наблюдалось широкое черенковское кольцо. Используя точную и приближенные формулы, мы рассмотрели, как излучает заряд, равномерно движущийся в среде на конечном интервале. Точные формулы справедливы во всем пространстве, внутри и вне кольца. В плоскости, перпендикулярной оси движения, излучение сосредоточено главным образом в кольце конечных размеров. Ширина этого кольца и энергия, в нем выделяемая, не зависят от положения плоскости наблюдения. Вне кольца интенсивность излучения резко падает. Небольшие осцилляции внутри кольца возникают из-за интерференции черенковского и тормозного излучений. Усиление интенсивности излучения на границах кольца обязано ударным волнам, возникающим в начале и в конце движения и в те моменты, когда скорость заряда совпадает со скоростью света в веществе. Внутри кольца известная формула Тамма не описывает интенсивность излучения ни при каком положении плоскости наблюдения. Вне кольца формула Тамма справедлива только на очень больших расстояниях плоскости наблюдения. Теоретические расчеты находятся в удовлетворительном согласии с экспериментальными данными. Мы заключаем: совместное (экспериментальное и теоретическое) изучение несфокусированных черенковских колец позволяет получить информацию о процессах, сопровождающих черенковское излучение (тормозное излучение, излучение, возникающее при прохождении светового барьера, и т. д.).

Работа выполнена в Лаборатории теоретической физики им. Н. Н. Боголюбова и в Лаборатории ядерных проблем им. В. П. Джелепова ОИЯИ.

Препринт Объединенного института ядерных исследований. Дубна, 2003

Afanasiev G. N., Kartavenko V. G., Zrelov V. P. E3-2003-83
On the Fine Structure of the Vavilov–Cherenkov Radiation

The aim of this paper is to study the fine structure of the Cherenkov rings. We analyze Zrelov's experiments in which the Cherenkov radiation was detected without using the special focusing devices. The broad Cherenkov ring was observed in the plane perpendicular to the motion axis. Using the exact and approximate formulae, we investigate how a charge uniformly moving in medium radiates in a finite space interval. The formulae obtained describe the radiation intensity in the whole space interval, inside and outside the Cherenkov ring. In the plane perpendicular to the motion axis, the radiation fills mainly the finite ring. Its width, proportional to the motion interval, and the energy released in this ring do not depend on the position of the observation plane. Outside the Cherenkov ring, the radiation intensity suddenly drops. Inside it, the radiation intensity exhibits small oscillations which are due to the interference of the Vavilov–Cherenkov radiation and bremsstrahlung. The increase in the radiation intensity at the ends of the Cherenkov ring is associated with the shock waves arising at the beginning and the end of the charge motion and at the moments when the charge velocity coincides with the light velocity in medium. For the chosen motion interval, the well-known Tamm formula does not describe the radiation intensity inside the Cherenkov ring for any position of the observation plane. Outside the Cherenkov ring, the Tamm formula is valid only at very large observation distances. Theoretical calculations are in satisfactory agreement with experimental data. Thus, the combined experimental and theoretical study of the unfocused Cherenkov rings allows one to obtain information on the physical processes accompanying the Cherenkov radiation (bremsstrahlung, transition of the light velocity barrier, etc.).

The investigation has been performed at the Bogoliubov Laboratory of Theoretical Physics and at the Dzhelepov Laboratory of Nuclear Problems, JINR.

Preprint of the Joint Institute for Nuclear Research. Dubna, 2003

Макет *Т. Е. Попеко*

Подписано в печать 03.06.2003.
Формат 60 × 90/16. Бумага офсетная. Печать офсетная.
Усл. печ. л. 1,68. Уч.-изд. л. 2,56. Тираж 415 экз. Заказ № 53935.

Издательский отдел Объединенного института ядерных исследований
141980, г. Дубна, Московская обл., ул. Жолио-Кюри, 6.
E-mail: publish@pds.jinr.ru
www.jinr.ru/publish/